WAVESHAPING WITH NORTON AMPLIFIERS: MODELING THE SERGE TRIPLE WAVESHAPER

Geoffrey Gormond *

Phelma
Grenoble Institute of Technology
Grenoble, France

Fabián Esqueda, Henri Pöntynen

Dept. of Signal Processing and Acoustics
Aalto University
Espoo, Finland

Julian D. Parker

Native Instruments GmbH
Berlin, Germany

ABSTRACT

The Serge Triple Waveshaper (TWS) is a synthesizer module designed in 1973 by Serge Tcherepnin, founder of Serge Modular Music Systems. It contains three identical waveshaping circuits that can be used to convert sawtooth waveforms into sine waves. However, its sonic capabilities extend well beyond this particular application. Each processing section in the Serge TWS is built around what is known as a Norton amplifier. These devices, unlike traditional operational amplifiers, operate on a current differencing principle and are featured in a handful of iconic musical circuits. This work provides an overview of Norton amplifiers within the context of virtual analog modeling and presents a digital model of the Serge TWS based on an analysis of the original circuit. Results obtained show the proposed model closely emulates the salient features of the original device and can be used to generate the complex waveforms that characterize "West Coast" synthesis.

1. INTRODUCTION

In the early 1970s, during the heyday of companies like Moog, ARP, and Buchla, access to modular synthesizers was mostly restricted to renowned musicians and members of the academic community. In those days a decently-equipped modular synthesizer, such as the Moog System 55[1], could easily cost tens of thousands of dollars. Frustrated by the high price tags of these instruments, Serge Tcherepnin, a then-professor of music composition at California Institute of the Arts (CalArts) decided to design a modular synthesizer that would be both affordable and powerful. With the support of a few CalArts students and faculty members, Serge set up a scheme in which people would pay $700 up front for parts and work on an improvised assembly line building their own six-module system [1, 2]. Serge's synthesizers became so successful that in 1975 he decided to leave his teaching position at CalArts to found *Serge Modular Music Systems*.

Since the beginning, Serge's approach to synthesizer design was heavily inspired by the work of Don Buchla on what is now known as "West Coast" synthesis. West Coast synthesis explored the use of non-traditional interfaces, such as step sequencers, and focused on timbre manipulation at waveform level via some form of nonlinear waveshaping [3]. In particular, Serge proposed expanding the signal path used in traditional subtractive synthesis by adding a "Wave Processor" stage between the oscillator and the voltage-controlled filter (VCF) [1]. Modules such as the Serge Wave Multipliers (VCM) [4], and the Triple Waveshaper (TWS) were designed for this purpose.

In this work we study the internal design of the Serge TWS module and propose a model for its digital implementation. The TWS is a processing module designed in 1973 as part of the first generation of Serge modules. As explained by Rich Gold[2] in his book *An Introduction to the Serge Modular Music System*, "the TWS module contains three identical devices which can be used to convert sawtooth waves into sine waves and can provide a wide range of other forms of sound and timbre modification. The timbre can be affected by a manual pot and two different VC inputs which operate on the sound in two different ways. It is a useful module for producing interesting and changing sound timbres, something difficult to achieve in other synthesizers" [5].

The motivation behind this study is to provide a better understanding of the Serge TWS, of which there is very little information available in the public domain, and to produce a "virtual analog" (VA) model that can be incorporated into a software-based synthesis environment. VA modeling is a popular area of study dedicated to emulating the behavior of vintage analog audio devices in the digital domain. This is highly desirable partly because nearly fifty years later, vintage analog synthesizers are still prohibitively expensive and hard to have access to. In a way, the motivation behind this kind of research is not much different from that of Serge Tcherepnin's when he started designing musical instruments.

Previous research on VA modeling of synthesizer circuits has concentrated on VCFs [6, 7, 8, 9, 10], oscillators [11, 12, 13], and effects processors [4, 14, 15]. Of related interest to this study is the pioneering work done during the 1970s on digital waveshaping synthesis [16, 17, 18]. This type of synthesis (much like West Coast synthesis) exploited the use of nonlinear waveshaping, e.g., via Chebyshev polynomials, to create harmonically-rich sounds from sinusoidal waveforms. These techniques are, in turn, closely related to popular digital synthesis methods such as frequency modulation and phase distortion synthesis [19, 20], which also relied on spectral manipulation via attribute modulation.

This paper is organized as follows. Section 2 provides an overview of Norton amplifiers, the component around which the module is based. Section 3 focuses on the analysis of the Serge TWS circuit. In Section 4 we observe the time- and frequency-domain behavior of the proposed model. Finally, Section 5 provides concluding remarks.

* Correspondence related to this work should be addressed to geoffrey.gormond@gmail.com

[1] https://www.moogmusic.com/products/modulars/system-55

[2] Rich Gold was part of the group of CalArts affiliates who worked on the design of the first Serge synthesizers. He was also responsible for the design of many of the emblematic Serge panels, which featured geometrical shapes instead of text labels [1].

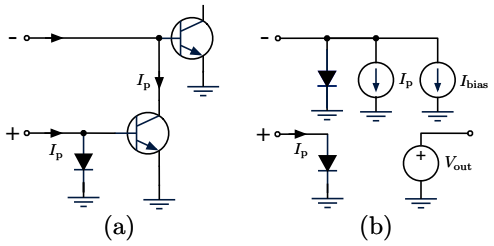

Figure 1: Circuit diagram for (a) the input stage and (b) a simplified equivalent circuit of a typical Norton amplifier. Figures adapted from [22].

2. NORTON AMPLIFIERS

Whereas the output voltage of the common operational amplifier is proportional to the voltage difference across its input terminals, the output of a Norton amplifier is proportional to the difference in the currents flowing into its input terminals [21]. Accordingly, Norton amplifiers are said to operate on a current differencing principle. This functionality is achieved by replacing the typical differential opamp input stage with a transistor configuration employing a current mirror at the positive input terminal to drain current from the negative input terminal, as shown in Fig. 1(a). As a first large-signal approximation, and as suggested in [22], a Norton amplifier can be modeled by the circuit shown in Fig. 1(b). Here, the transistor at the negative input terminal has been abstracted to a single base–emitter junction diode. Similarly, the current mirror has been reduced to a diode at the positive terminal and a current source that drains a replica of the positive input current from the negative terminal. A bias current source is added to the negative terminal and the output is represented as a voltage source that depends on the input currents. When negative feedback is applied, the output of the device settles at a voltage that minimizes the current difference between the input terminals [23]. This behavior is similar to that of conventional op-amps that seek to minimize the voltage difference across the inputs under negative feedback.

In typical applications, the diode at the negative input terminal remains forward biased if the small bias current $I_{\text{bias}} = 30\,\text{nA}$ is supplied to the negative input. Usually, this current is available when negative feedback is applied. The diode associated with the current mirror at the positive input terminal is commonly biased separately with a resistive connection to the power supply [24, 25]. With the diodes forward biased, the input terminals of the device are clamped to a diode drop above ground potential and the input pins can be treated as fixed voltage nodes. This fixed voltage assumption is the basis for many of the circuit design equations associated with Norton amplifiers [22, 23].

Compared to voltage-differencing operational amplifiers, Norton amplifiers are relatively uncommon devices in audio applications. Nevertheless, iconic vintage devices, such as VCFs in ARP synthesizers [26, 27], were designed around the LM3900; an integrated circuit housing four identical Norton amplifiers. This–now obsolete–device was favored by circuit designers for various applications due to its compactness, low cost and robust operation with a wide range of unipolar supply voltages. For instance, the LM3900 is capable of nearly full output voltage swings from approximately ground level (around 90 mV) to one diode drop below the supply voltage while maintaining stability [22]. The device even played a hidden role in shaping the sound aesthetics of video games, as the sound effects and the iconic background loop in the hit arcade game *Space Invaders* were implemented with dedicated synthesis circuits designed around the LM3900 [28]. Moreover, the LM3900 is particularly abundant in the designs of Serge Tcherepnin, who employed it widely to implement a variety of his synthesizer modules (e.g., the dual universal slope generator [3], the smooth & stepped generator [4], the bottom section of the VCM [5], a touch responsive keyboard [6], envelope generators [7], and many more). In the next section, we present a circuit analysis of the Serge TWS, an audio processor where the LM3900 was employed in an unconventional manner to perform complex waveshaping.

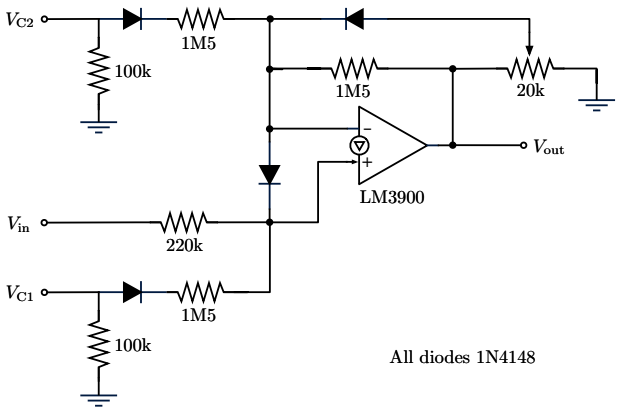

Figure 2: Circuit diagram for a single stage of the Serge TWS module. Figure adapted from [29].

3. THE SERGE TWS

Figure 2 shows a simplified schematic of a single stage of the Serge TWS [29]. The circuit takes a single input signal and applies a static waveshaping function to it. Control voltages V_{C1} and V_{C2} are then used to change the shape of this function. Figure 3(a) shows the model of the circuit used in this study. Here, we have substituted the LM3900 for the large-signal model described in Section 2. Additionally, the circuitry associated with the control voltage inputs V_{C1} and V_{C2} has been collapsed into ideal current sources I_A and I_B, respectively, both of which range from 0–3 μA. The range of these current sources was based on the standard used in Serge synthesizers, which expects DC-coupled and AC-coupled (i.e. audio) signals to range between approximately 0–5 V and ± 2.5 V, respectively. The blue diodes in Fig. 3(a) represent the BJT base–emitter junctions inside the LM3900, while the red diodes represent standard 1N4148 silicon signal diodes.

We divide the analysis of the circuits in two parts. First, we look at the input section and compute the value of currents I_p and I_f. Once these currents are known we proceed to analyze the feedback portion of the circuit and the output section. These steps are detailed in the following subsections.

[3] www.cgs.synth.net/modules/cgs114_dusg.html
[4] www.cgs.synth.net/modules/cgsssg_ssg.html
[5] www.cgs.synth.net/modules/cgs113_vcm.html
[6] www.cgs.synth.net/modules/cgs86_trk.html
[7] www.cgs.synth.net/modules/cgs76_env.html

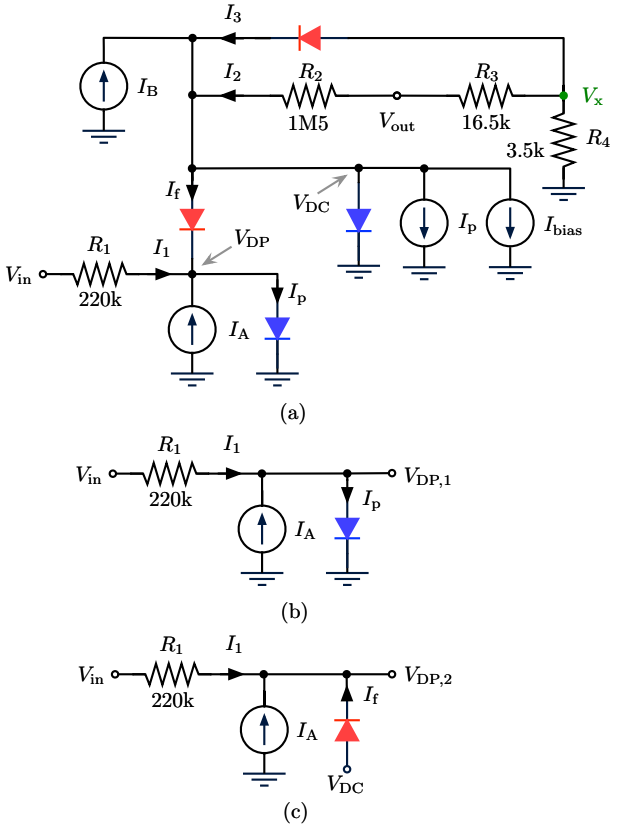

Figure 3: Circuit diagram for (a) the large signal model of a single stage of the Serge TWS and (b)–(c) the two subcircuits at the negative and positive terminals of the LM3900 amplifier, respectively. Blue and red diodes represent BJT base–emitter junction diodes and 1N4148 silicon diodes, respectively.

3.1. Input Section

We begin our analysis by computing the value of currents I_p and I_f. By applying Kirchhoff's current law (KCL) at the node labeled V_{DP} in Fig. 3(a) we can establish that

$$I_1 = I_p - I_f - I_A. \tag{1}$$

Next, we make the assumption that when either of the two diodes in the input section conducts, the contribution of the other one to the total value of I_1 will be close to zero. Therefore, we can analyze the two subcircuits shown in Figs. 3(b) and 3(c) independently. This approach will allow us to explicitly calculate I_p and I_f separately at each input sample without introducing discontinuities or significant errors in the model. As discussed in the previous section, we assume that the internal biasing in the Norton amplifier together with the application of negative feedback ensures that the diode inside the negative terminal is always forward-biased. This means that we can treat it as a fixed voltage node that we define to be clamped at $V_{DC} = 516\,\text{mV}$ based on SPICE simulations.

For the subcircuit in Fig. 3(b), we apply Kirchhoff's voltage law (KVL) and KCL to establish that

$$V_{in} = R_1 I_1 + V_{DP,1} \tag{2}$$
$$I_1 = I_P - I_A, \tag{3}$$

where I_p can be written using Shockley's diode equation as

$$I_p = I_{s,1}\left(\exp\left(\frac{V_{DP,1}}{\eta_1 V_T}\right) - 1\right), \tag{4}$$

where parameters $I_{s,1}$, η_1 and V_T represent the reverse bias saturation current, ideality factor and thermal voltage (at room temperature) of an ideal base–emitter p–n junction, respectively. All of the parameters required to implement the proposed model are given in Table 1. The tabulated semiconductor parameters were obtained from the LM3900 datasheet [22] and SPICE component models. By combining (2) and (3) with (4), we arrive at the implicit relationship

$$V_{DP,1} = V_{in} + R_1 I_A - R_1 I_{s,1}\left(\exp\left(\frac{V_{DP,1}}{\eta_1 V_T}\right) - 1\right), \tag{5}$$

which has the explicit solution

$$V_{DP,1} = V_{in} + R_1 I_A + R_1 I_{s,1} - \eta_1 V_T \mathrm{W}\left(\frac{R_1 I_{s,1}}{\eta_1 V_T}\exp\left(\frac{V_{in} + R_1 I_A + R_1 I_{s,1}}{\eta_1 V_T}\right)\right), \tag{6}$$

where $W(\,)$ is the Lambert-W function. The use of the Lambert-W function to solve the implicit current-voltage relationship of diodes was first proposed in [30], and extended in [31] and [32].

This same procedure can be followed for the subcircuit in Fig. 3(c), which gives us the explicit formulation

$$V_{DP,2} = V_{in} + R_1 I_A - R_1 I_{s,2} + \eta_2 V_T \mathrm{W}\left(\frac{R_1 I_{s,2}}{\eta_2 V_T}\exp\left(\frac{V_{DC} + R_1 I_{s,2} - V_{in} - R_1 I_A}{\eta_2 V_T}\right)\right), \tag{7}$$

where $I_{s,2}$ and η_2 are the reverse bias saturation current and ideality factor of the 1N4148 silicon diode, respectively. Once the value of $V_{DP,2}$ is known, the current I_f can be evaluated as

$$I_f = I_{s,2}\left(\exp\left(\frac{V_{DC} - V_{DP,2}}{\eta_2 V_T}\right) - 1\right). \tag{8}$$

Figure 4 shows the value of currents I_p and I_f computed using (4) and (8), respectively. Both currents are plotted against measurements obtained from a SPICE simulation (gray lines) of the large-signal model in Fig. 3(a). These results indicate our previous assumptions do not alter the overall general behavior of the model.

Table 1: *Component/parameter values.*

Name	Value	Name	Value
R_1	220 kΩ	$I_{s,2}$	2.52 nA
R_2	1.5 MΩ	η_1	1
R_3	16.5 kΩ	η_2	1.752
R_4	3.5 kΩ	V_T	25.864 mV
R_5	1 kΩ	V_{DC}	516 mV
$I_{s,1}$	10^{-14} A	I_{bias}	30 nA

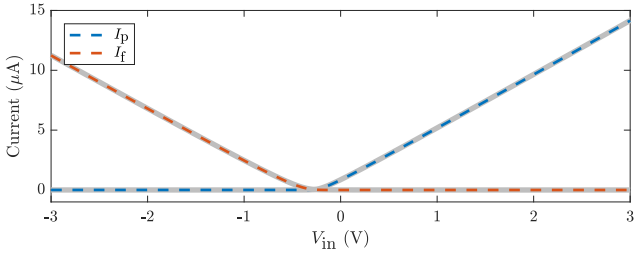

Figure 4: Value of I_p and I_f as a function of V_{in} computed using the proposed model and plotted against SPICE measurements (light gray lines).

3.2. Feedback Section

Having computed currents I_p and I_f we can analyze the feedback section of the circuit and derive a closed-form expression for V_{out}. As before, we apply KVL and KCL at the node labeled V_{DC} to derive the relationships

$$V_{out} = R_2 I_2 + V_{DC} \tag{9}$$

$$I_2 = I_f + I_p + I_{bias} - I_B - I_3, \tag{10}$$

where $I_{bias} = 30\,\text{nA}$ [22] and

$$I_3 = I_{s,2}\left(\exp\left(\frac{V_x - V_{DC}}{\eta_2 V_T}\right) - 1\right). \tag{11}$$

Here, V_x (highlighted in green in Fig. 3(a)) represents the voltage at the wiper node of the potentiometer in Fig. 2. Combining (11) with (9) and (10) gives us

$$V_{out} = V_{DC} + R_2 I_G - R_2 I_{s,2}\left(\exp\left(\frac{V_x - V_{DC}}{\eta_2 V_T}\right) - 1\right), \tag{12}$$

where the substitution $I_G = (I_f + I_p + I_{bias} - I_B)$ has been used for clarity. Similarly, applying KVL and KCL at V_x we arrive at the expression

$$V_{out} = R_3 I_{s,2}\left(\exp\left(\frac{V_x - V_{DC}}{\eta_2 V_T}\right) - 1\right) + G V_x, \tag{13}$$

where $G = (R_3/R_4 + 1)$. If we then equate (12) and (13), and solve for V_x, we arrive at the implicit expression for the wiper voltage

$$V_x = \frac{V_{DC} + R_2 I_G}{G} - \frac{R_2 + R_3}{G}\left(\exp\left(\frac{V_x - V_{DC}}{\eta_2 V_T}\right) - 1\right), \tag{14}$$

which can be solved using the Lambert-W function as

$$V_x = \frac{V_{DC} + R_2 I_G + (R_2 + R_3) I_{s,2}}{G} - \eta_2 V_T \mathrm{W}\left(\frac{(R_2 + R_3) I_{s,2}}{G \eta_2 V_T} \times \exp\left(\frac{-V_{DC}}{\eta_2 V_T}\right) \exp\left(\frac{V_{DC} + R_2 I_G + (R_2 + R_3) I_{s,2}}{G \eta_2 V_T}\right)\right). \tag{15}$$

This expression can be used to compute the value of V_x which can then be used to compute the value of V_{out} by evaluating either (12) or (13).

3.3. Output Clipping

As explained in Section 2, the LM3900 operates on a single power supply and is unable to generate voltages below approximately 90 mV. Therefore, this behavior must be accounted for in the proposed model. For the sake of simplicity, we propose an ad hoc approach that involves emulating the clipping behavior with a piecewise nonlinear function. We introduce a new voltage variable $\widetilde{V}_{out}$ which represents the value of the output voltage after clipping. The expression for the proposed clipper can be written as

$$\widetilde{V}_{out} = \begin{cases} V_{clip} & V_{out} \leq V_{clip} \\ V_{clip}\sqrt{1 + (\frac{V_{out}}{V_{clip}} - 1)^2} & \text{otherwise} \end{cases} \tag{16}$$

where $V_{clip} = 90\,\text{mV}$.

3.4. Model Summary

Having derived all the necessary expressions, in this section we provide a summary of the steps required to emulate the circuit in the digital domain. Since the circuit is static, we can compute the output directly by assuming a discrete-domain input signal $V_{in}[n]$, where n is the sample index. The steps required to compute $\widetilde{V}_{out}[n]$ are:

1. Evaluate voltages $V_{DP,1}[n]$ and $V_{DP,2}[n]$ using (6) and (7), respectively.
2. Compute currents $I_p[n]$ and $I_f[n]$ using (4) and (8).
3. Evaluate voltage $V_x[n]$ using (15).
4. Evaluate $V_{out}[n]$ using either (12) or (13).
5. Apply the clipping function (16).

Figures 5(a) and 5(b) show the input–output relationship of the circuit for different values of I_A evaluated using the proposed model and with SPICE, respectively. This comparison indicates a good match between the proposed model and its corresponding SPICE simulation, with a maximum difference of approximately 22 mV, as shown in Fig. 5(c). As shown in these figures, the system exhibits a highly nonlinear behavior which resembles that of a soft clipper cascaded with a full-wave rectifier. Adjusting the value of I_A changes the x-axis symmetry of the circuit.

Similarly, the plots in Figures (6)(a) and (6)(b) show the effect of increasing control current I_B from 0 to 3 μA. This parameter appears to "open" or "widen" the shape of the nonlinearity. The clipping behavior of the LM3900 is evident in these plots. Once again, the proposed model shows a good match with its corresponding SPICE simulation, with a maximum difference of approximately 70 mV (cf. Fig. (6)(c)). This increased difference can be attributed to the ad hoc modeling of the clipping stage.

Finally, the curves in Figures 7(a) and 7(b) shows the measured input–output relationship of a real Serge TWS built according to the schematic given in Fig. 2. The behavior of the circuit was measured for different values of control voltages V_{C1} and V_{C2}. When compared with Figs. 5(b) and 6(b), these results further demonstrate the proposed model preserves the salient characteristics of the circuit.

3.5. AC Coupling

The plots in Figures 5 and 6 show that the output of the Serge TWS will exhibit a static DC offset. The original circuit solved this by providing an additional AC-coupled output [29]. This is

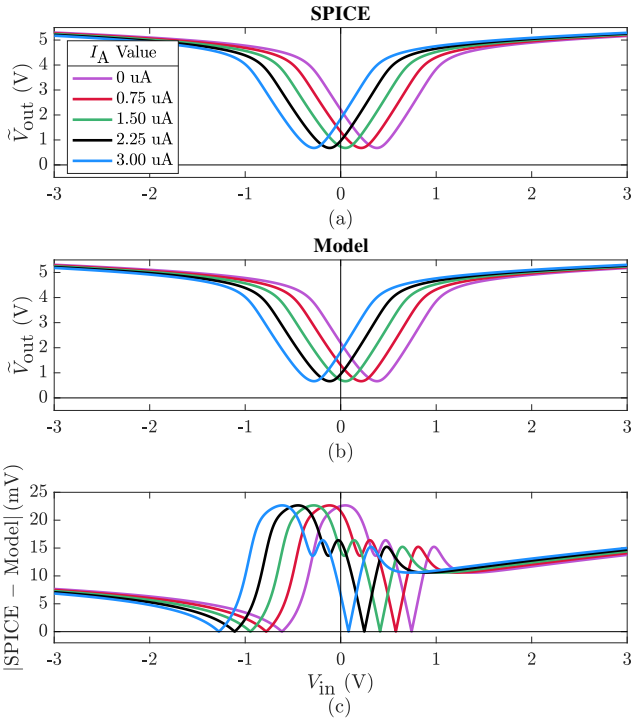

Figure 5: Input–output relationship of a single stage in the Serge TWS for values of I_A between 0–3 μA ($I_B = 0$ A) simulated using (a) SPICE and (b) the proposed model, and (c) the absolute value of the difference between both sets of curves.

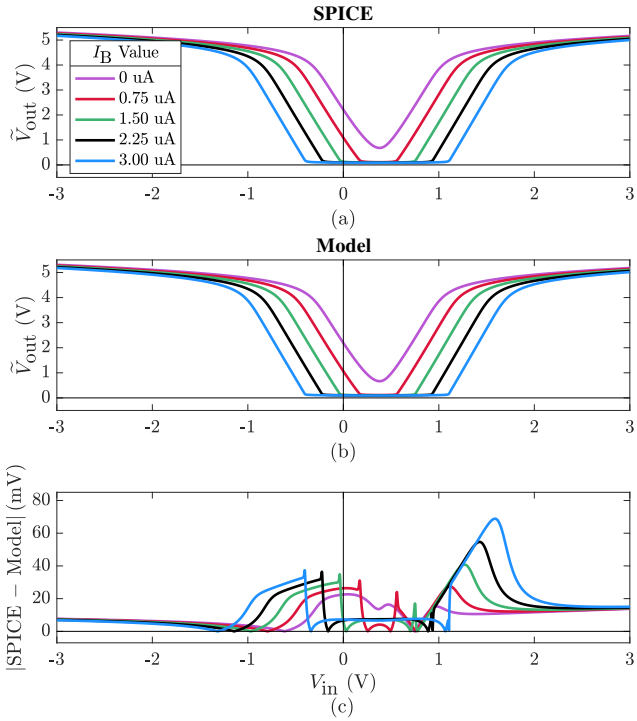

Figure 6: Input–output relationship of the system for values of I_B between 0–3 μA ($I_A = 0$ A) simulated using (a) the digital model and (b) SPICE, and (c) the absolute value of their difference.

quite typical in Serge modules as they were designed to process not only audio signals but also control voltages, which must be DC-coupled. In the digital domain, an AC-coupled version of the output can be computed, for instance, by using the first-order DC blocker proposed by Pekonen and Välimäki in [33]. The z-domain transfer function of this filter is defined as

$$H_{DC}(z) = \frac{1+p}{2}\frac{1-z^{-1}}{1-pz^{-1}}, \tag{17}$$

where $p = \tan(\pi/4 - \pi f_c/F_s)$, F_s is the sampling rate of the system and f_c is the cut-off frequency of the filter, set at 2 Hz in this case.

4. RESULTS

In this section we examine the time- and frequency-domain behavior of the circuit when driven by sawtooth waveforms, as recommended in the original user manual [5]. Figure 8 shows the output of a single stage of the Serge TWS when driven by an 80-Hz sawtooth waveform with peak amplitude of 1 V for different values of I_A when $I_B = 0$. The resulting waveforms have been stacked on top of each other to help visualize the evolution of the output signal as a function of I_A. To minimize the effects of aliasing, the original input waveform (shown in blue at the top of the plot) was synthesized using the first-order differentiated parabolic waveform (DPW) algorithm at a sampling rate $F_s = 352.8$ kHz (i.e. 8-times oversampling w.r.t. standard audio rate) [13]. This sample rate is used throughout the rest of this study. From this figure we can observe that the circuit does indeed transform the input waveform into something that resembles a sine wave. The best results are obtained when $I_A \approx 1.5\,\mu$A, as the circuit exhibits near-perfect even symmetry (cf. Fig. 5).

This case is presented in greater detail in Figs. 9(c)–(d) which

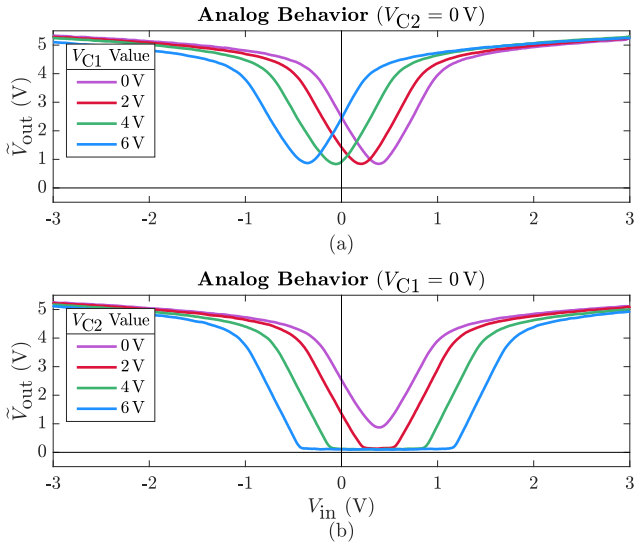

Figure 7: Measured analog input–output behavior of the circuit in Fig. 2 for different values of V_{C1} and V_{C2}.

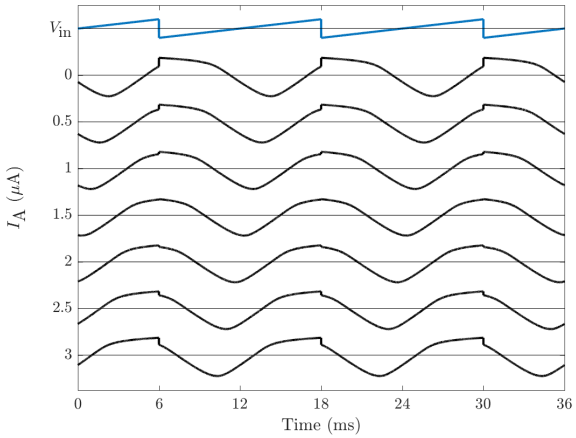

Figure 8: Output of the proposed model when driven by an 80-Hz sawtooth waveform for different values of I_{A} ($I_{\text{B}} = 0$).

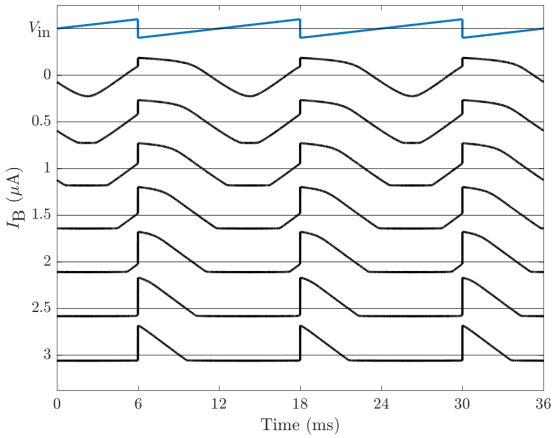

Figure 10: Output of the proposed model when driven by an 80-Hz sawtooth waveform for different values of I_{B} ($I_{\text{A}} = 0$).

show the waveform and magnitude spectrum of a 200-Hz sawtooth waveform with peak amplitude of 1 V processed by the model for $I_{\text{A}} = 1.5\,\mu$A. These results show that, as originally advertised, the circuit can indeed approximate a sinusoidal waveform when driven by a 1-V sawtooth signal. Although the resulting waveform shows a strong presence of the second harmonic, nearly all other partials have been significantly attenuated. However, this behavior is heavily dependent on the level of the input signal. Figures 9(e)–(f) show the result of driving the proposed model with a 2.5-V sawtooth waveform. In this case the resulting waveform no longer resembles a sine wave, as it exhibits considerably high harmonic content. As a reference, Figs. 9(a)–(b) present the waveform and magnitude spectrum of the 200-Hz sawtooth input.

Next, we consider the effect of control current I_{B} on the output. Figure 10 shows the output of the Serge TWS when driven by a 80-Hz sawtooth waveform with peak amplitude of 1 V for different values of I_{B} when $I_{\text{A}} = 0$. As shown in these plots, increasing the value of I_{B} increases the amount of clipping introduced by the circuit. These results go in accordance with the the input–output relationship of the model (cf. Fig 6). Lastly, Fig. 11 shows the recorded analog response of the circuit when driven by an 80-Hz sawtooth signal under different settings. These results further validate the accuracy of the proposed model, as they match the waveforms depicted in Figs. 8–9. The measured waveforms were normalized during the recording process.

We observe the frequency domain behavior of the system by considering the spectrograms in Figs. 12 and 13. The first spectrogram shows the effect of varying control current I_{A} linearly for a static 500-Hz sawtooth input (peak amplitude of 1 V). We can once again observe the region of values of I_{A} for which the waveshaper approximates a sinusoidal output. Overall, this behavior contrasts

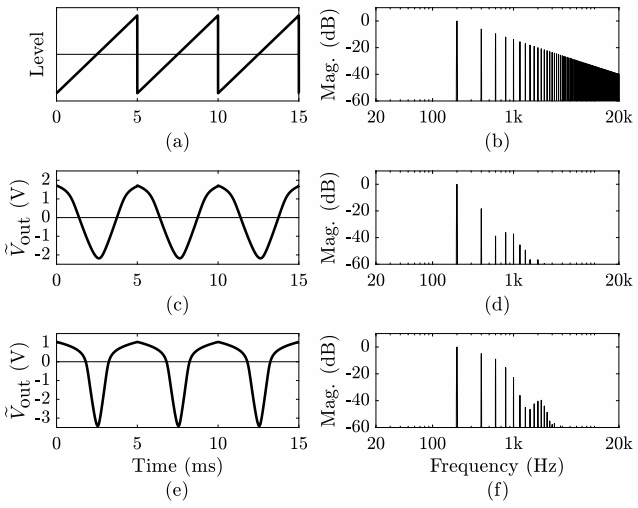

Figure 9: Waveform and magnitude spectrum of (a)–(b) a 200-Hz sawtooth, (c)–(d) a 1-V and (e)–(f) a 2.5-V sawtooth processed by the proposed model. Parameters $I_{\text{A}} = 1.5\,\mu$A and $I_{\text{B}} = 0$ A.

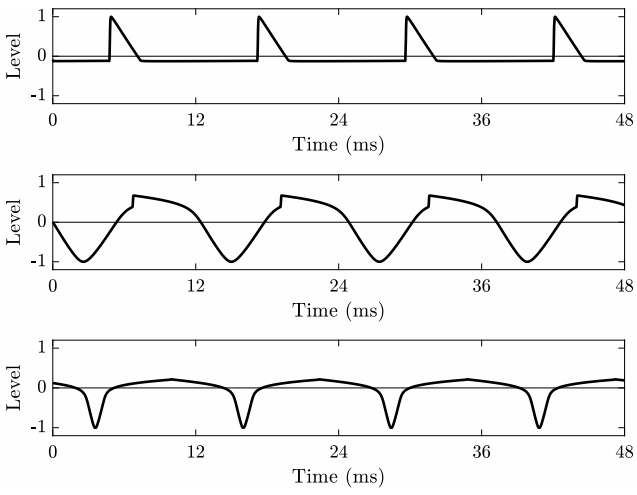

Figure 11: Measured analog time-domain behavior of a single stage in the Serge TWS when driven by an 80-Hz analog sawtooth waveform for different values of V_{C1} and V_{C2} (cf. Fig. 2).

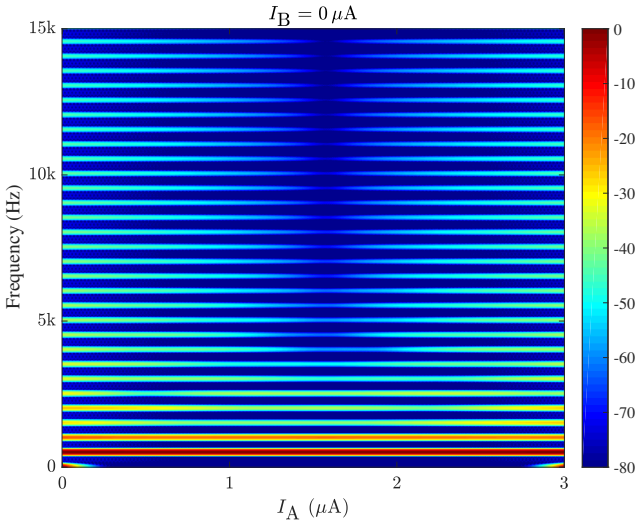

Figure 12: Magnitude response of a single stage in the Serge TWS when driven by a 1-V 500-Hz sawtooth waveform for values of I_A between 0–3 μA and $I_B = 0$ A.

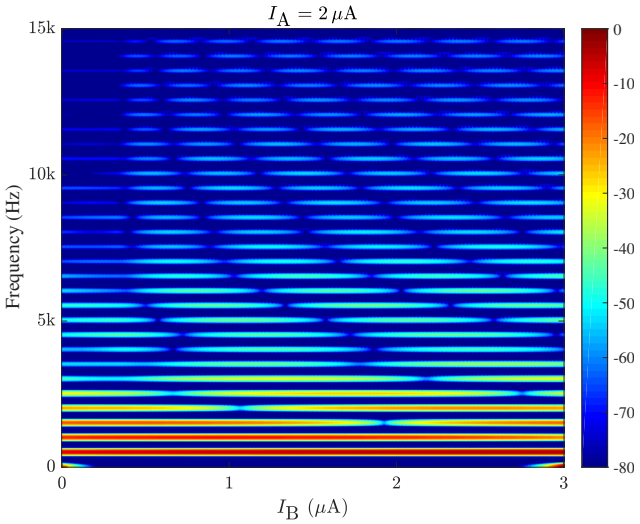

Figure 13: Magnitude response of a single stage in the Serge TWS when driven by a 1-V 500-Hz sawtooth waveform for $I_A = 2\,\mu$A and values of I_B between 0–3 μA.

that of other Serge circuits, such as the middle section of the VCM which is designed to expand the frequency content of sinusoidal waveforms [4]. The second spectrogram shows the effect of modulating I_B for a static value of $I_A = 2\,\mu$A. This value was chosen as it displayed interesting and complex harmonic patterns.

Finally, we briefly consider what happens when the three identical waveshapers in the Serge TWS are connected in series. This form of usage of the circuit is so popular that some re-issues of the module (e.g. the Random*Source Serge Triple+ Waveshaper[8]) even feature integrated switches to link the stages internally. Figure 14 shows the output waveforms that result from processing an 80-Hz sawtooth waveform (peak amplitude 2.5 V) using three stages in cascade. Control parameters I_A and I_B where kept constant between stages. The DC blocker (17) was used in between each stage. As shown in these plots, the cascaded configuration no longer operates as originally intended. Nevertheless, it can be used to produce the complex waveforms that characterize West Coast synthesis.

Overall, the sonic possibilities offered by the Serge TWS are quite vast. By manipulating all free input parameters, i.e. input level and control currents, different timbral effects can be achieved. When all three stages are cascaded, the number of combinations increases even further, as the parameters of each stage can be modulated independently. Sound articulation and timbral variety are then achieved by modulating the control currents in real-time. It should also be noted that the use of the circuit is not restricted to sawtooth signals. It can be used to process virtually any input waveform regardless of its harmonic nature. This makes the Serge TWS an extremely powerful and versatile synthesis tool.

5. CONCLUSIONS

In this work we examined the underlying structure of the Serge TWS module. We introduced Norton amplifiers and discussed the use of a simplified large-signal model for their emulation in the digital domain. A digital model of a single waveshaping stage in the module was proposed. The model was validated against a SPICE simulation of the same circuit. Results from driving the proposed model with multiple sawtooth waveforms show the Serge TWS can be used to transform sawtooth signals into sinusoidal waveforms, but can also be used to generate highly complex signals with interesting harmonic patterns. This study provides an insight into Serge Tcherepnin's approach to synthesis and opens the door for further study of his iconic circuits. Supplementary materials for this paper can be found in the accompanying website `http://research.spa.aalto.fi/publications/papers/dafx18-serge-tws`.

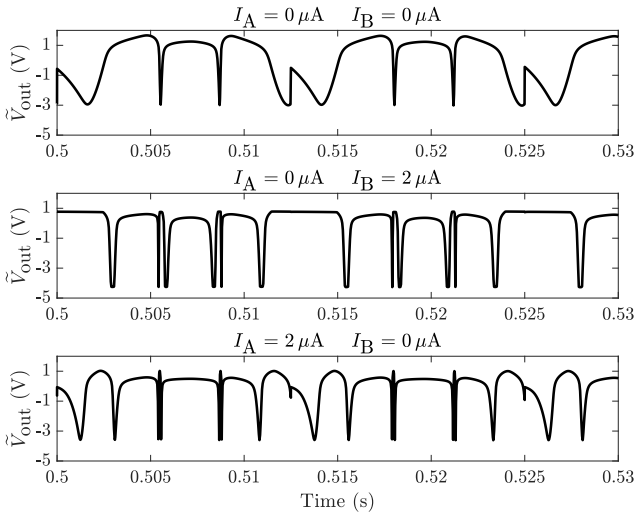

Figure 14: Results of processing an 80-Hz sawtooth waveform using three waveshapers arranged in series. The values of I_A and I_B used for these simulations are indicated on top of each subplot.

[8] `http://randomsource.net/serge_euro`

6. ACKNOWLEDGMENTS

The authors would like to thank Ken Stone and Serge Tcherepnin for the valuable correspondence during the early stages of this project. The main part of this work was conducted during Geoffrey Gormond's visit to Aalto University in summer 2017.

7. REFERENCES

[1] M. Vail, "Serge Modular Systems: Maximum Analog Horsepower," in *Vintage Synthesizers*, M. Vail, Ed., pp. 147–152. Miller Freeman Books, San Francisco, CA, USA, 2000.

[2] L. Mizzell, "Serge Modular Music Systems – Historical Bits and Pieces," Available online: `http://www.serge-fans.com/history.htm` (accessed 11 April 2018).

[3] J. Parker and S. D'Angelo, "A digital model of the Buchla lowpass-gate," in *Proc. Int. Conf. Digital Audio Effects (DAFx-13)*, Maynooth, Ireland, Sept. 2013.

[4] F. Esqueda, H. Pöntynen, J. D. Parker, and S. Bilbao, "Virtual analog models of the Lockhart and Serge wavefolders," *Appl. Sci.*, vol. 7, no. 12, Dec. 2017.

[5] R. Gold, D. Johansen, and M. LaPalma, "An Introduction to the Serge Modular Music System," Available online: `http://serge.synth.net/documents/` (accessed 11 April 2018).

[6] D. Rossum, "Making digital filters sound analog," in *Proc. Int. Comput. Music Conf.*, San Jose, CA, USA, Oct. 1992, pp. 30–33.

[7] A. Huovilainen, "Non-linear digital implementation of the Moog ladder filter," in *Proc. Int. Conf. Digital Audio Effects (DAFx-04)*, Naples, Italy, Oct. 2004, pp. 61–64.

[8] F. Fontana and M. Civolani, "Modeling of the EMS VCS3 voltage-controlled filter as a nonlinear filter network," *IEEE Trans. Audio, Speech, Language Process.*, vol. 18, no. 4, pp. 760–772, Apr. 2010.

[9] S. D'Angelo and V. Välimäki, "Generalized Moog ladder filter: Part II–explicit nonlinear model through a novel delay-free loop implementation method," *IEEE/ACM Trans. Audio, Speech, Language Process.*, vol. 22, no. 12, pp. 1873–1883, Dec. 2014.

[10] M. Rest, J. Parker, and K. J. Werner, "WDF modeling of a Korg MS-50 based non-linear diode bridge VCF," in *Proc. Int. Conf. Digital Audio Effects (DAFx-17)*, Edinburgh, UK, Sept. 2017, pp. 61–164.

[11] T. Stilson and J. Smith, "Alias-free digital synthesis of classic analog waveforms," in *Proc. Int. Comput. Music Conf.*, Hong Kong, Aug. 1996, pp. 332–335.

[12] E. Brandt, "Hard sync without aliasing," in *Proc. Int. Comput. Music Conf.*, Havana, Cuba, Sept. 2001, pp. 365–368.

[13] V. Välimäki, J. Nam, J. O. Smith, and J. S. Abel, "Alias-suppressed oscillators based on differentiated polynomial waveforms," *IEEE Trans. Audio Speech Lang. Process.*, vol. 18, no. 4, pp. 786–798, May 2010.

[14] F. Esqueda, H. Pöntynen, V. Välimäki, and J. D. Parker, "Virtual analog Buchla 259 wavefolder," in *Proc. Int. Conf. Digital Audio Effects (DAFx-17)*, Edinburgh, UK, Sept. 2017, pp. 61–164.

[15] J. Parker, "A simple digital model of the diode-based ring modulator," in *Proc. Int. Conf. Digital Audio Effects (DAFx-11)*, Paris, France, Sept. 2011, pp. 163–166.

[16] R. A. Schaefer, "Electronic musical tone production by nonlinear waveshaping," *J. Audio Eng. Soc.*, vol. 18, no. 4, pp. 413–417, 1970.

[17] D. Arfib, "Digital synthesis of complex spectra by means of multiplication of nonlinear distorted sine waves," *J. Audio Eng. Soc.*, vol. 27, no. 4, pp. 757–768, 1979.

[18] M. Le Brun, "Digital waveshaping synthesis," *J. Audio Eng. Soc.*, vol. 27, pp. 250–266, 1979.

[19] J. M. Chowning, "The synthesis of complex audio spectra by means of frequency modulation," *J. Audio Eng. Soc.*, vol. 21, no. 7, pp. 526–534, 1973.

[20] M. Ishibashi, "Electronic musical instrument," Patent No. 4,658,691, 21 April 1987.

[21] M. F. Hribšek and D. V. Tošić, "Symbolic analysis and design of current-differencing-amplifier filters," *Scientific Technical Review*, vol. 57, no. 2, pp. 19–23, 2007.

[22] National Semiconductor Corporation, *The LM3900: A New Current-Differencing Quad of ± Input Amplifiers*, Application Note 72. Sept. 1972.

[23] D. J. Dailey, *Electronics for Guitarists*, Springer, New York City, NY, USA, 2nd edition, 2012.

[24] R. Marston, "Understanding and using 'Norton' op-amps ICs – part 1," *Nuts and Volts*, vol. 23, no. 7, pp. 51–54, July 2002.

[25] R. Marston, "Understanding and using 'Norton' op-amps ICs – part 2," *Nuts and Volts*, vol. 23, no. 8, pp. 49–53, Aug. 2002.

[26] ARP Instruments, Inc., "4072 Voltage-Controlled Low-pass Filter," Available online: `http://www.yusynth.net/Modular/EN/ARPVCF/index.html` (accessed 15 April 2018).

[27] ARP Instruments, Inc., "Dynamic filter," 1977.

[28] M. Mera, R. Sadoff, and B. Winters, *The Routledge Companion to Screen Music and Sound*, Routledge, Abingdon, UK, 1st edition, 2017.

[29] K. Stone, "Triple wave shaper for music synthesizers," Available online: `https://www.cgs.synth.net/modules/cgs85_tws.html` (accessed 21 March 2018).

[30] T. Banwell and A. Jayakumar, "Exact analytical solution for current flow through diode with series resistance," *Electron. Lett.*, vol. 36, no. 4, pp. 291–292, Feb. 2000.

[31] R. C. D. de Paiva, S. D'Angelo, J. Pakarinen, and V. Välimäki, "Emulation of operational amplifiers and diodes in audio distortion circuits," *IEEE Trans. Circuits Syst. II, Exp. Briefs*, vol. 59, no. 10, pp. 688–692, Oct. 2012.

[32] K. J. Werner, V. Nangia, A. Bernardini, J. O. Smith III, and A. Sarti, "An improved and generalized diode clipper model for wave digital filters," in *Proc. 139th Conv. Audio Eng. Soc.*, New York, USA, Oct.–Nov. 2015.

[33] J. Pekonen and V. Välimäki, "Filter-based alias reduction for digital classical waveform synthesis," in *Proc. Int. Conf. Acoustics, Speech and Signal Processing(ICASSP)*, Las Vegas, NV, USA, Mar.–Apr. 2008, pp. 133–136.